Inorganic Chemistry

ARTICLE

pubs.acs.org/IC

New Series of Triply Bridged Dinuclear Cu(II) Compounds: Synthesis, Crystal Structure, Magnetic Properties, and Theoretical Study

Nanthawat Wannarit,[†] Khatcharin Siriwong,[†] Narongsak Chaichit,[‡] Sujittra Youngme,*[,†] Ramon Costa,[§] Ibério de P. R. Moreira,[⊥] and Francesc Illas*[,⊥]

[†]Department of Chemistry and Center of Excellence for Innovation in Chemistry, Faculty of Science, Khon Kaen University, Khon Kaen 40002, Thailand

[‡]Department of Physics, Faculty of Science and Technology, Thammasat University Rangsit, Pathumthani 12121, Thailand

[§]Departament de Química Inorgànica and Institut de Química Teòrica i Computacional (IQTCUB), Universitat de Barcelona, C/Martí i Franquès 1, E-08028 Barcelona, Spain

[⊥]Departament de Química Física and Institut de Química Teòrica i Computacional (IQTCUB), Universitat de Barcelona, C/Martí i Franquès 1, E-08028 Barcelona, Spain

Supporting Information

ABSTRACT: Five new triply bridged dinuclear Cu(II) compounds have been synthesized, and their magnetic properties have been measured and characterized. The magnetic coupling constants (J) of these compounds plus a previously structurally characterized compound of the same type have been derived by appropriate fitting of the experimentally measured molar susceptibility variation with the temperature. Two of the compounds are ferromagnetically coupled, and three are antiferromagnetically coupled with J values in the $[+150, -40]$ cm^{-1} range. The validity of the structural aggregate Addison's parameter as a qualitative magneto-structural correlation is confirmed. The origin of the magnetic interactions and the magnitude of the magnetic coupling have been analyzed by means of density functional theory-based calculations using a variety of state of the art exchange-correlation potentials. It is shown that the long-range separated LC-ωPBE provides the overall best agreement with experiment for this family as well as for a set of previously reported hetero triply bridged dinuclear Cu(II) compounds, especially for ferromagnetic systems.

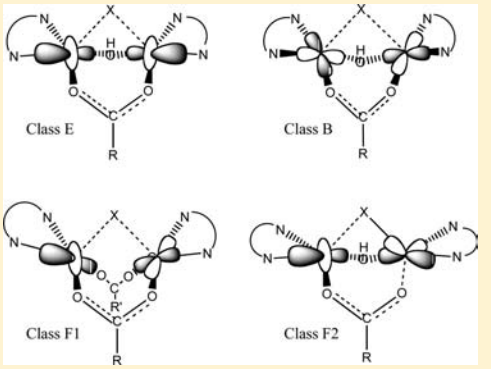

INTRODUCTION

The study of magnetochemistry in di- and polynuclear Cu(II) coordination compounds is of interest due to the diverse structural and magnetic properties of these systems and, especially, because of the possibility to design structures exhibiting strong ferromagnetism. The design, synthesis, and magnetic characterization of these types of systems is still challenging. In addition, this family of systems is usually presented as representative of the simplest possible models for magnetic complexes since the Cu(II) ions in a d^9 electronic configuration exhibit only one unpaired electron per magnetic center. This feature allows one to search for a deeper understanding of ferro- and antiferromagnetic interactions and to derive useful magneto-structural correlations from either experimental or theoretical points of view which provide a guide toward magnetic complexes with enhanced ferromagnetism.[1,2]

This work follows from previous research focusing on the dinuclear triply bridged copper(II) compounds which have shown to exhibit a great diversity of topologies, intramolecular magnetic exchange phenomena, and magneto-structural correlations.[3−8] In these compounds, the five coordination of the Cu(II) ion displays an extensive range of distorted geometries ranging from regular trigonal bipyramid to regular square-based pyramid. Their global topologies can be described in terms of the relative arrangement of the two five-coordinate environments, giving rise to different classes of compounds termed A to F in previous work.[3] The knowledge of these topologies is useful to unravel the relationships between structural features and the value of the intramolecular magnetic exchange interaction in the triply bridged dinuclear unit. In the previously mentioned study, the magneto-structural correlations were investigated with the help of semiempirical Extended Hückel calculations and linear correlations were found for class B compounds.[3] However, a more quantitative approach is needed to fully understand the magnetic interactions in these compounds and to accurately predict their magnetic coupling constant J. More recently, a deep investigation on the magneto-structural correlations in this series of compounds, which show ferromagnetic behavior, was carried out[9] using density functional theory (DFT)-based calculations. Results have shown that for class B compounds the calculated magnetic coupling constant values almost quantitatively correlate with the sum of Addison's τ parameter of each Cu(II) ion. This class provides a clear example of enhanced ferromagnetic

Received: May 11, 2011
Published: September 26, 2011

Scheme 1

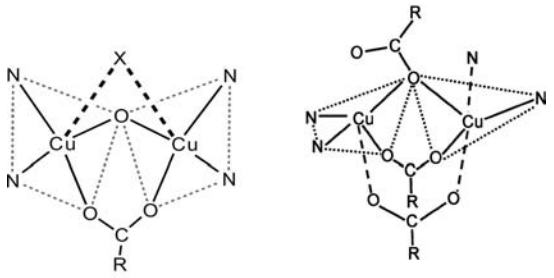

behavior using ligands favoring the square-based pyramidal coordination on each Cu(II) atom which involves magnetic interaction mainly through the Cu(II) $d_{x^2-y^2}$ orbitals. On the other hand, calculated *J* values for class E compounds reveal that a third ligand plays a key role in enhancing ferromagnetism in this class which involves mainly the interaction through the Cu(II) d_{z^2} orbitals.

To extend our knowledge on the magnetic behavior and the magneto-structural correlations of these triply bridged dinuclear compounds with different topologies (Scheme 1), we successfully synthesized two new hetero triply bridged dinuclear Cu(II) compounds in class B $\{[Cu_2(phen)_2(\mu\text{-}OH)(\mu\text{-}OH_2)(\mu\text{-}O_2CC(CH_3)_3)](ClO_4)_2\}_2(CH_3CH_2OH)$ (**1**) and $[Cu_2(bpy)_2(\mu\text{-}OH)(\mu\text{-}O_2CCH_2CH_3)(\mu\text{-}O_2SOCF_3)](CF_3SO_3)(DMF)_{0.5}$ (**2**); we also consider one structurally reported[3] class B compound $[Cu_2(phen)_2(\mu\text{-}OH)(\mu\text{-}OH_2)(\mu\text{-}O_2CCH_2CH_3)](NO_3)_2$ (**3**). From the existing literature, it appears that the number of class F compounds for which both structural and magnetic data is available is found to be very limited. Hence, three new homo triply bridged dinuclear Cu(II) compounds in class F, $[Cu_2(bpy)_2(\mu\text{-}OCOPh)(\mu\text{-}O_2CPh)_2]X$ with X = ClO_4^-(**4**), BF_4^- (**5**), and PF_6^- (**6**) have been synthesized and characterized. Details of the synthesis, characterization, and crystal structure of the new compounds are reported. Also, values of the magnetic coupling constants extracted from magnetic susceptibility measurements are compared to theoretical calculations using a wide range of state of the art DFT methods including the newest range-separated hybrid functionals. Incorporating the present systems to previously published ferromagnetic triply bridged di-Cu(II) compounds allows us to propose a more complete open-shell database which may be very useful to systematically investigate the performance of newly developed exchange-correlation functionals in predicting magnetic coupling constants in these and more complicated magnetic systems as well as to generalize an important previously reported magnetostructural correlation for triply bridged di-Cu(II) complexes.[9]

MATERIALS AND MEASUREMENTS

1,10-Phenanthroline, 2,2′-bipyridine, sodium trimethylacetate monohydrate, sodium propionate, and sodium benzoate were purchased as commercial chemicals from Aldrich. All reagents are commercial grade materials and were used without further purification. Elemental analyses (C, H, N) were determined using a Perkin-Elmer PE-2400 CHNS/O Analyzer.

IR spectra were recorded on Spectrum One FT-IR spectrophotometer as KBr disk in the 4000−450 cm^{-1} spectral range. Solid-state (diffuse reflectance) electronic spectra were measured as polycrystalline samples on a Perkin-Elmer Lambda2S spectrophotometer, over the range 8000−18000 cm^{-1}.

Magnetic susceptibility measurements for compounds **1**−**6** were carried out on polycrystalline samples at the *Servei de Magnetoquímica* of the *Serveis Científico-Tècnics* of the *Universitat de Barcelona*. They were carried out with a Quantum Design SQUID MPMS-XL magnetometer working in the temperature range 2−300 K at magnetic fields of 500 G (2−30 K) and 10 kG (2−300 K). For compounds **1** and **3**, due the small amounts of available samples (30 and 60 mg, respectively), the measurements were repeated twice. Diamagnetic corrections for the measured susceptibilities were estimated from the Pascal tables. The EPR spectra of microcrystalline samples of **1**−**6** were recorded at X-band frequency ($\nu \sim 9.4362$ GHz) with a Bruker ES-200 spectrometer in the temperature range 300−4 K.

Synthesis. *$\{[Cu_2(phen)_2(\mu\text{-}OH)(\mu\text{-}OH_2)(\mu\text{-}O_2CC(CH_3)_3)](ClO_4)_2\}_2(CH_3CH_2OH)$ (**1**).* A warm ethanol solution (25 mL) of phen (0.198 g, 1.0 mmol) was added to a warm aqueous solution (15 mL) of $Cu(ClO_4)_2\cdot 6H_2O$ (0.370 g, 1.0 mmol). Then, $(CH_3)_3CCO_2Na$ solid (0.124 g, 1.0 mmol) was added to the mixture, yielding a clear dark blue solution. After 1 week, bluish-violet rectangle-shaped crystals of compound **1** were obtained. The crystals were filtered off, washed with mother liquor, and air-dried. Yield: ca. 30%. Anal. Calc. for $Cu_4C_{60}H_{60}N_8O_{25}Cl_4$: C, 42.66; H, 3.59; N, 6.64. Found: C, 42.12; H, 3.51; N, 6.66%.

*$[Cu_2(bpy)_2(\mu\text{-}OH)(\mu\text{-}O_2CCH_2CH_3)(\mu\text{-}O_2SOCF_3)](CF_3SO_3)(DMF)_{0.5}$ (**2**).* A warm aqueous solution (5 mL) of $Cu(CF_3SO_3)_2$ (0.361 g, 1.0 mmol) was added to a mixed methanol and DMF (20:3) solution of bpy (0.156 g, 1.0 mmol). Then, $CH_3CH_2CO_2Na$ solid (0.096 g, 1.0 mmol) was added to the mixture, yielding a clear blue solution. After 1 week, bluish-violet hexagonal shaped crystals of compound **2** were obtained. The crystals were filtered off, washed with mother liquor, and air-dried. Yield: ca. 60%. Anal. Calc. for $Cu_2C_{26.5}H_{25.5}N_{4.5}O_{9.5}S_2F_6$: C, 36.82; H, 2.98; N, 7.29. Found: C, 36.25; H, 2.86; N, 7.20%.

*$[Cu_2(phen)_2(\mu\text{-}OH)(\mu\text{-}OH_2)(\mu\text{-}O_2CCH_2CH_3)](NO_3)_2$ (**3**).* Compound **3** was synthesized by the method described previously in ref 3. Yield: ca. 30%. Anal. Calc. for $Cu_2C_{27}H_{24}N_6O_{10}$: C, 45.07; H, 3.36; N, 11.68. Found: C, 45.01; H, 3.25; N, 11.83%.

*$[Cu_2(bpy)_2(\mu\text{-}OCOPh)(\mu\text{-}O_2CPh)_2](ClO_4)$ (**4**) and $[Cu_2(bpy)_2(\mu\text{-}OCOPh)(\mu\text{-}O_2CPh)_2](BF_4)$ (**5**).* The warm aqueous solution (10 mL) of $Cu(ClO_4)_2\cdot 6H_2O$ (0.370 g, 1.0 mmol) was added to a warm methanol solution (20 mL) of bpy (0.156 g, 1.0 mmol). Then, solid $C_6H_5CO_2Na$ (0.144 g, 1.0 mmol) was added to the mixture, yielding a clear greenish-blue solution. After 1 week, greenish-blue hexagonal shaped crystals of compound **4** were obtained. The crystals were filtered off, washed with mother liquor, and air-dried. Yield: ca. 65%. Anal. Calc. for $Cu_2C_{41}H_{31}N_4O_{10}Cl_1$: C, 54.57; H, 3.47; N, 6.21. Found: C, 54.28; H, 3.38; N, 6.78. %. Compound **5** was prepared in similar manner using $Cu(BF_4)_2\cdot nH_2O$. Yield: ca. 70%. Anal. Calc. for $Cu_2C_{41}H_{31}N_4O_6BF_4$: C, 55.35; H, 3.52; N, 6.30. Found: C, 55.24; H, 3.32; N, 6.38%.

*$[Cu_2(bpy)_2(\mu\text{-}OCOPh)(\mu\text{-}O_2CPh)_2](PF_6)$ (**6**).* The warm aqueous solution (10 mL) of $Cu(NO_3)_2\cdot 3H_2O$ (0.241 g, 1.0 mmol) was added to a warm methanol solution (20 mL) of bpy (0.156 g, 1.0 mmol). Then, solid $C_6H_5CO_2Na$ (0.144 g, 1.0 mmol) was added to the mixture. After that, solid of KPF_6 or $(NH_4)PF_6$ (2.0 mmol) was added, yielding a clear greenish-blue solution. After 1 week, greenish-blue hexagonal shaped crystals of compound **6** were obtained. The crystals were filtered off, washed with mother liquor, and air-dried. Yield: ca. 60%. Anal. Calc. for $Cu_2C_{41}H_{31}N_4O_6PF_6$: C, 51.95; H, 3.30; N, 5.91. Found: C, 51.75; H, 3.13; N, 6.08%.

Crystallography. X-ray single-crystal data for all compounds were collected at 293 K. Reflection data were collected on a 1K Bruker SMART APEX CCD area-detector diffractometer using rotating mode, graphite-monochromated Mo Kα radiation (λ = 0.71073 Å) at a detector distance of 4.5 cm and swing angle of −30°. A hemisphere of the reciprocal space was covered by combination of three sets of exposures; each set had a different ϕ angle (0°, 88°, 180°), and each exposure of 40 s covered 0.3° in ω. Raw data frame integration was performed with SAINT,[10] which also applied correction for Lorentz and

Table 1. Crystallographic and Refinement Data for Compounds 1, 2, and 4−6[a]

Compound	1	2	4	5	6
Empirical formula	$Cu_4N_8C_{60}H_{60}O_{25}Cl_4$	$Cu_2N_{4.5}C_{26.5}H_{25.5}O_{9.5}S_2F_6$	$Cu_2N_4C_{41}H_{31}O_{10}Cl_1$	$Cu_2N_4C_{41}H_{31}O_6B_1F_4$	$Cu_2N_4C_{41}H_{31}P_1F_6$
Formula weight	1689.28	864.30	902.31	889.67	947.83
T/K	293(2)	293(2)	293(2)	293(2)	293(2)
Crystal system	triclinic	monoclinic	monoclinic	monoclinic	monoclinic
Space group	P-1	$C2/c$	$P2_1/c$	$P2_1/c$	$P2_1/c$
a (Å)	8.8313(2)	28.9098(11)	11.48420(10)	11.526(2)	11.5546(2)
b (Å)	18.8577(6)	14.4295(6)	21.6488(3)	21.490(4)	22.31590(10)
c (Å)	20.5115(6)	17.6698(7)	15.9640(4)	15.927(3)	15.9854(2)
α (°)	90.1850(10)	90.00	90.00	90.00	90.00
β (°)	94.0770(10)	115.3140(10)	109.6090(10)	109.23(3)	109.9900(10)
γ (°)	96.4580(10)	90.00	90.00	90.00	90.00
V (Å^3)	3385.46(17)	6663.2(5)	3738.77(11)	3725.0(13)	3873.52(8)
Z	2	4	4	4	4
D_{calc} (g cm^{-3})	1.632	1.694	1.603	1.586	1.625
μ (mm^{-1})	1.483	1.493	1.277	1.217	1.223
$F(000)$	1690	3420	1840	1808	1920
Crystal size (mm)	0.08 × 0.13 × 0.20	0.05 × 0.23 × 0.40	0.38 × 0.38 × 0.55	0.28 × 0.33 × 0.43	0.10 × 0.13 × 0.35
Number of reflection collected	15972	24886	28002	9471	27590
Number of unique reflections (R_{int})	10870 (0.0290)	9673 (0.0351)	10619 (0.0193)	5095 (0.0161)	10756 (0.0423)
Data/restraints/parameter	10870/1/936	9673/10/463	10619/0/684	5095/2/683	10756/0/701
Goodness-of-fit	1.013	1.062	1.050	1.027	0.888
Final R indices [$I > 2\sigma(I)$]	R_1 = 0.0612	R_1 = 0.0810	R_1 = 0.0313	R_1 = 0.0307	R_1 = 0.0388
	wR_2 = 0.1558	wR_2 = 0.2670	wR_2 = 0.0859	wR_2 = 0.0795	wR_2 = 0.0791
R indices (all data)	R_1 = 0.1144	R_1 = 0.1392	R_1 = 0.0469	R_1 = 0.0406	R_1 = 0.0993
	wR_2 = 0.1815	wR_2 = 0.3083	wR_2 = 0.0905	wR_2 = 0.0862	wR_2 = 0.0934
Largest difference in peak and hole (e^3)	1.062 and −0.679	2.638 and −0.892	0.319 and −0.743	0.300 and −0.517	0.316 and −0.523

[a] $R = \Sigma||F_o| - |F_c||/\Sigma|F_o|$, $R_w = [\Sigma w\{||F_o| - |F_c||\}^2/\Sigma w|F_o|^2]^{1/2}$.

Polarization effects. An empirical absorption correction using the SADABS[11] program was applied, which resulted in transmission coefficients ranging from 1.000 to 0.678, 1.000 to 0.761, 1.000 to 0.747, 1.000 to 0.809, and 1.000 to 0.749 for **1**, **2**, and **4**−**6**. The structures were solved by direct methods and refined by full-matrix least-squares method on $(F_{obs})^2$ using the SHELXTL-PC Version 6.12 software package.[12]

For compound **1**, all hydrogen atoms were introduced in calculated positions and refined with fixed geometry with respect to their carrier carbon atoms except those of hydroxo bridges, H(1A) and H(5A), and water bridging molecules, H(2A), H(6A), and H(7A), while a hydrogen atom of one water bridging molecule and an ethanol molecule could not be located. All nonhydrogen atoms were refined anisotropically. The Cl(4)−O(22) bond distance of perchlorate group was restrained with the DFIX 1.45(1) command. An ethanol molecule was disordered with site occupancies of 0.5. In compound **2**, all hydrogen atoms were introduced in calculated positions and refined with fixed geometry with respect to their carrier carbon atoms except hydrogen atoms of the hydroxo bridge and DMF molecule. All nonhydrogen atoms were refined anisotropically, except some atoms of noncoordinated triflate anion. For bridging triflate, the oxygen atoms of SO_3 group were disordered with site occupancies of 0.5. The triflate counteranion was disordered, and attempts have been made to locate disordered atoms in a range of reasonable possibilities but were unsuccessful. Finally, we decide to refine as the ordered molecule and it was restrained to the bond distance with the DFIX 1.42(1), 1.86(1), and 1.32(1) commands for the S−O, C−S, and C−F, respectively, leading to quite high but reliable temperature factors. The free DMF molecule was also disordered and restrained of the bond distance with the DFIX 1.23(1), 1.35(1), and 1.47(1) commands for the C(31)−O(17), N(6)−C(31), and N(6)−C(32), respectively. For compound **4**, all hydrogen atoms were located by difference synthesis and refined isotropically, while all nonhydrogen atoms were refined anisotropically. The perchlorate anion was disordered with site occupancies of oxygen atoms of 0.52 and 0.48. In compound **5**, all hydrogen atoms were located by difference synthesis and refined isotropically, while all nonhydrogen atoms were refined anisotropically. The tetrafluoroborate molecule was disordered with site occupancies of 0.5, and it was restrained with the DFIX 1.34(1) Å, for the B(1)−F(1) and B(1)−F(1A) bond lengths. Finally, for compound **6**, all hydrogen atoms were located by difference synthesis and refined isotropically except a hydrogen atom, H(7), on pyridine ring of bpy and those of benzoate bridging ligands, H(25), H(37), H(38), and H(40). All nonhydrogen atoms were refined anisotropically. The tetrafluoroborate molecule is disordered with site occupancies of 0.5.

Computational Details. The different series of hybrid DFT calculations have been carried out using rather large standard basis sets of Gaussian Type Orbitals (GTO). Thus, a 6-3111+G extended with an f-function (exponent(f) = 0.528) has been used for Cu and 6-31G(d) for the remaining atoms. All calculations have been carried out in the unrestricted (spin-polarized) formalism. Clearly, in this type of formalism, the spin symmetry is not guaranteed.[13−15] Nevertheless, approximate triplet (T) states have been obtained from the unrestricted Kohn−Sham formalism using a single Slater determinant with two unpaired electrons (i.e., $S_z = 1$) whereas to estimate the energy of the open shell singlet state we have relied on the broken-symmetry (BS) approach imposing $S_z = 0$. In this way, the singlet−triplet gap energy has been obtained on the basis of the expectation value of the Heisenberg Hamiltonian as in eq 1

$$\hat{H} = -J\,\hat{\mathbf{S}}_1\cdot\hat{\mathbf{S}}_2 \qquad (1)$$

dx.doi.org/10.1021/ic200992z |Inorg. Chem. 2011, 50, 10648–10659

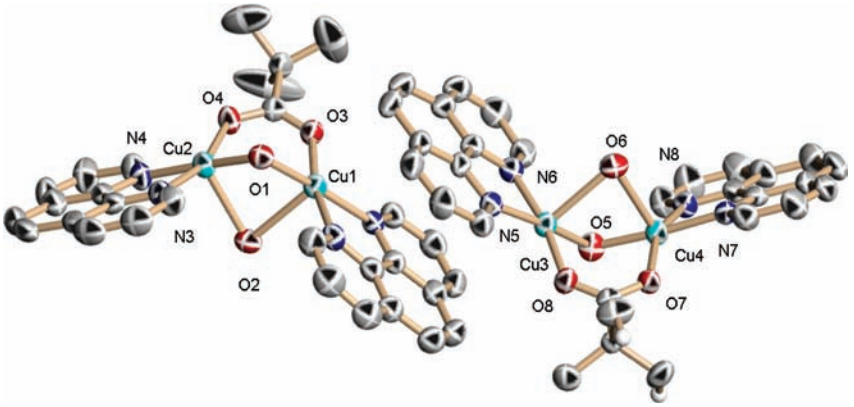

Figure 1. Two independent dinuclear Cu(II) cationic units and atomic numbering scheme for compound **1** (Thermal ellipsoids are shown at 30% level). Hydrogen atoms, perchlorate anions, and ethanol molecules are omitted for clarity.

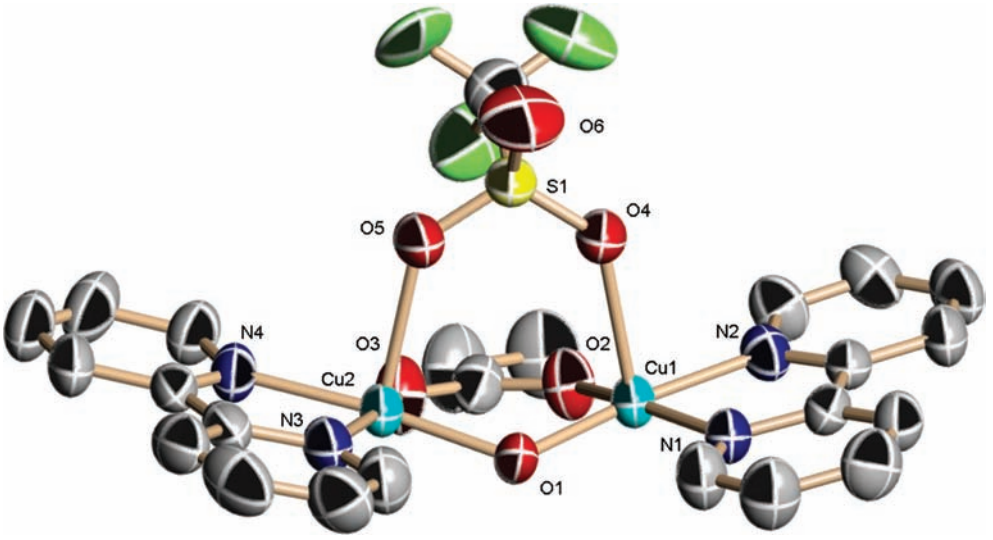

Figure 2. Molecular structure and atomic numbering scheme for compound **2** (Thermal ellipsoids are shown at 50% level). Hydrogen atoms, triflate counteranions, and DMF molecule are omitted for clarity.

that leads to the approximate relation:

$$J = 2[E(\mathrm{BS}) - E(\mathrm{T})] \quad (2)$$

where $E(\mathrm{BS})$ is the energy of the broken-symmetry state and $E(\mathrm{T})$ is the energy of the spin unrestricted approximation to the triplet state.[16] Here, it is important to stress that eq 2 takes into account the so-called spin projection, which aims to recover the spin symmetry lost in the BS approach and which is inherent to the use of a single Kohn−Sham determinant.[17−19] Alternative methods for calculating J couplings without the use of spin symmetry[20] lead to results that are not always accurate[21] when high quality range separated functionals like those employed in this paper are used. All calculations were carried out using the Gaussian09 suite of programs.[22]

RESULTS AND DISCUSSION

The crystal structures and their refinement details for compounds **1**, **2**, and **4**−**6** are listed in Table 1. Selected bond lengths and angles are given in Tables 1−5 of the Supporting Information file which also contains a description of the crystal structures. Here, we just provide a very short description and hence mention that $\{[Cu_2(phen)_2(\mu\text{-}OH)(\mu\text{-}OH_2)(\mu\text{-}O_2CC(CH_3)_3)](ClO_4)_2\}_2(CH_3CH_2OH)$, hereafter referred to as compound **1**, has an asymmetric unit consisting of two independent triply bridged dinuclear Cu(II) units, four perchlorate counteranions, and one ethanol molecule (Figure 1). $[Cu_2(bpy)_2(\mu\text{-}OH)(\mu\text{-}O_2CCH_2CH_3)(\mu\text{-}O_2SOCF_3)](CF_3SO_3)(DMF)_{0.5}$, referred to as **2**, consists of a dinuclear $[Cu_2(bpy)_2(\mu\text{-}OH)(\mu\text{-}O_2CCH_2CH_3)(\mu\text{-}O_2SOCF_3)]^+$ cation, with trifluoromethanesulfonate counteranion and a half of DMF (Figure 2). $[Cu_2(phen)_2(\mu\text{-}OH)(\mu\text{-}OH_2)(\mu\text{-}O_2CCH_2CH_3)](NO_3)_2$, referred to as **3**, was described previously.[3] Dinuclear cations of compounds **1**, **2**, and **3** consist of two Cu(II) atoms each having a chelating bidentate terminal ligand and sharing three bridging ligands (one hydroxo, one carboxylato, and one water molecule for **1** and **3** and one triflate ligand for **2**) in such a way that a CuN_2O_3 chromophore defines a distorted square pyramidal pentacoordinated environment around the magnetic center with X atom in Scheme 1 at the apex of the SP. These three complexes are then classified as class B. On the other hand, $[Cu_2(bpy)_2(\mu\text{-}OCOPh)(\mu\text{-}O_2CPh)_2]X$ with X = ClO_4^- (**4**), BF_4^- (**5**), and PF_6^- (**6**) crystallize in the monoclinic space group $P2_1/c$ with similar unit cell parameters, as shown in Table 1. The structure of these compounds is similar to those described above except that the three bridging ligands are two bidentate and one monodentate carboxylates, leading to a distorted trigonal bi-

dx.doi.org/10.1021/ic200992z |*Inorg. Chem.* 2011, 50, 10648–10659

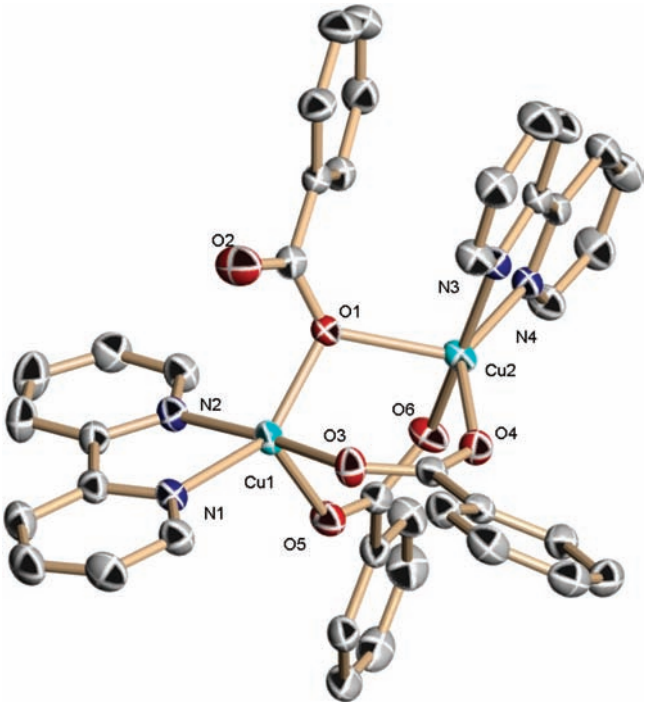

Figure 3. Molecular structure and atomic numbering scheme for compounds **4**−**6** (Thermal ellipsoids are shown at 30% level). Hydrogen atoms, perchlorate, tetrafluoroborate, and hexafluorophosphate anions for compounds **4**, **5** and **6** are omitted for clarity.

pyramidal geometry around the magnetic Cu(II) centers (Figure 3). According to the definition established in previous work,[9] compounds **4**, **5**, and **6** belong to class F (see Supporting Information). Note that the previously reported class F compound, $[Cu_2(dpyam)_2(\mu\text{-}OCOCH_3)(\mu\text{-}O_2CCH_3)(\mu\text{-}OH)](PF_6)(H_2O)$ (**XV**),[8] consists of two carboxylato and one hydroxo bridges. Due to the influence of these structural features in the magnetic behavior of the compounds, we will distinguish from now on between F1 (antiferromagnetic, one μ-(*O*,*O*)-carboxylato and two μ-(*O*,*O*′)-carboxylato bridges) and F2 (ferromagnetic, one hydroxo, and one μ-(*O*,*O*) and one μ-(*O*,*O*′) bridging carboxylates) classes, respectively.

Spectroscopic Features and Magnetic Characterization. *Infrared Spectra.* The infrared spectra display a broad band at 3504 cm^{-1} for **1** and 3567 cm^{-1} for **2**, which can be assigned to the bridging OH vibration of the hydroxo ligands and/or lattice water. The spectra also exhibit the intense bands at 1550 and 1424 cm^{-1} for **1** and 1542 and 1448 cm^{-1} for **2**, corresponding to the $\nu_{as}(COO^-)$ and $\nu_s(COO^-)$ vibrations of bridging trimethylacetate and propionate for **1** and **2**, respectively. Broad and intense bands of the stretching of $\nu_{as}(ClO_4)$ at 1096 cm^{-1} for **1** and $CF_3SO_3^-$ at 1260 ν_{as}(S−O), 1162 ν_{as}(C−F), 1032 ν_s(S−O), and 637 δ(S−O) cm^{-1} for **2** were observed. The IR spectra of compounds **4**−**6** present the broad and intense bands of the stretching for ionic ClO_4^- anion (1091 cm^{-1} for **4**), ionic BF_4^- anion (1056 cm^{-1} for **5**), and ionic PF_6^- anion (841 cm^{-1} for **6**).[23] The spectra of these compounds also show two broad and intense bands at 1567 and 1384 cm^{-1} for **4**, 1568 and 1385 cm^{-1} for **5**, and 1567 and 1383 cm^{-1} for **6**, corresponding to the $\nu_{as}(COO^-)$ and $\nu_s(COO^-)$ vibrations of benzoate bridging ligand.

uv−*Visible Spectra.* The diffuse reflectance spectra of compounds **1** and **2** display a broad band (16 000 cm^{-1} for **1** and 16 370 cm^{-1} for **2**) and a lower energy shoulder (13 140 cm^{-1} for **1** and 13 830 cm^{-1} for **2**). These features are typical and correspond to the d_{xy}, d_{yz}, $d_{xz} \rightarrow d_{x^2-y^2}$, and $d_{z^2} \rightarrow d_{x^2-y^2}$ transitions for the square pyramidal geometry of the triply bridged dinuclear copper(II) compounds.[3] However, the corresponding spectra for compounds **4**−**6** show a single broad band centered at ca. 11 930 for **4**, 11 900 for **5**, and 11 960 cm^{-1} for **6**, corresponding to an intermediate five-coordinate geometry.[24]

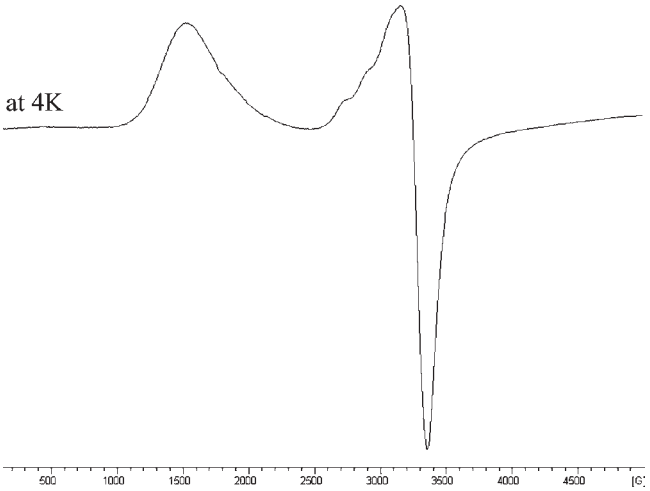

Figure 4. EPR spectrum of compound **1** at 4 K.

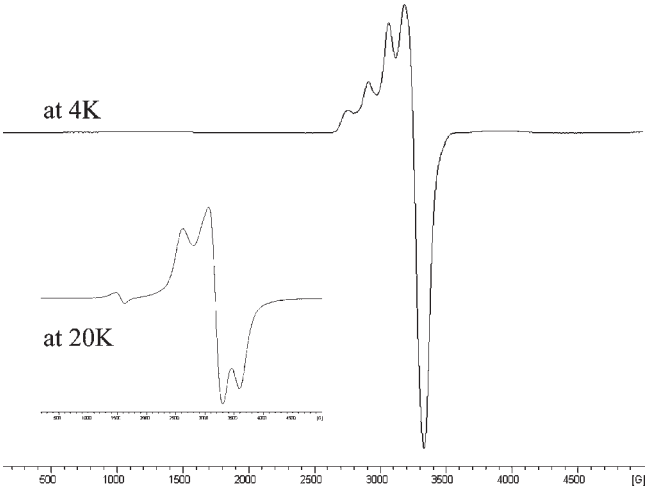

Figure 5. EPR spectrum of compound **4** at 4 K and at 20 K (see inset).

Electron Paramagnetic Resonance Spectra. The EPR spectra of the compounds **1**−**6** (X-band, $\nu \sim 9.4362$ GHz) have been recorded at different temperatures between 4 and 300 K for polycrystalline solid samples. The general shape of the spectra at 4 K corresponds to the two types shown in Figure 4 for ferromagnetic systems (compounds **1** to **3**) and in Figure 5 for antiferromagnetic systems (**4** to **6**).

In the case of ferromagnetic systems, the principal transition band near $g \sim 2.1$, corresponding to $\Delta m_s = 1$, shows some asymmetry but maintains the center of the band as T goes from 300 to 4 K, slightly increasing the intensity of the signals. The half field transition near $g \sim 4.4$, corresponding to $\Delta m_s = 2$, shows important intensity with respect to the $\Delta m_s = 1$ transition and

dx.doi.org/10.1021/ic200992z |*Inorg. Chem.* 2011, 50, 10648–10659

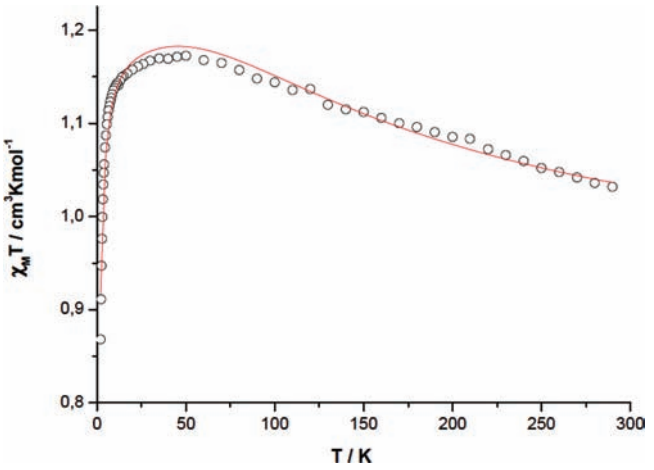

Figure 6. Plot of magnetic susceptibility−temperature product ($\chi_M T$) versus (T) temperature for compound **1**.

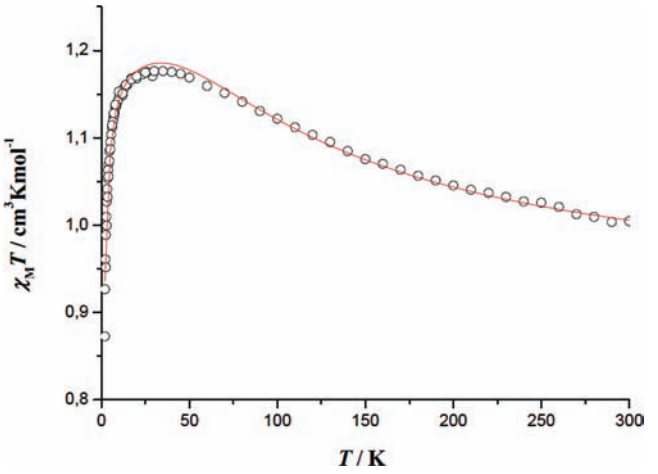

Figure 7. Plot of magnetic susceptibility−temperature product ($\chi_M T$) versus (T) temperature for compound **2**.

demonstrates that the signal is originated by an electronic triplet state. The fine structure is apparent at 4 K but to resolve it, even tentatively, goes well beyond the scope of the present work.

The spectra of the antiferromagnetic systems (compounds **4** to **6**) are quite different, and the shape is strongly dependent on the temperature: at 300 K, a broad symmetric doublet signal appears near $g \sim 2.1$ for $\Delta m_s = 1$ and the signal near $g \sim 4.4$ corresponding to $\Delta m_s = 2$ is almost unobservable. As temperature decreases, the main transition evolves to show an apparent fine structure and the half field transition for $\Delta m_s = 2$ becomes more intense and is very clear for temperatures around 20 K. Finally, when T approaches 4 K, the half field signal disappears and the principal signal at $g \sim 2.1$ becomes quite asymmetrical and shows a complex fine structure. The half field transition for $\Delta m_s = 2$ is observed, and its intensity increases as T decreases, reaches a maximum at intermediate temperatures, and disappears a low temperature. This behavior is consistent with a singlet−triplet electronic system with antiferromagnetic ground state and small J value.

Magnetic Properties. Molar magnetic susceptibility (χ_M) measurements were carried out using microcrystalline samples of compounds **1**−**6**. The $\chi_M T$ vs T plots for **1**−**3** (Figures 6, 7, and 8, respectively) show a room temperature $\chi_M T$ product value of 1.03, 1.00, and 0.97 cm^3Kmol^{-1} for **1**, **2**, and **3**, respectively, slightly higher to that expected for two uncoupled Cu(II) ions. Lowering the temperature causes the $\chi_M T$ product to continuously increase until reaching plateau values of 1.17 cm^3Kmol^{-1} at 50 K for **1**, 1.18 at 35 K for **2**, and 1.15 at 30 K for **3.** On further cooling, $\chi_M T$ shows an abrupt descent for the three compounds, which clearly suggests that this quantity tends to zero when temperature tends to 0 K. This behavior can be explained by the existence of ferromagnetically coupled Cu(II) pairs responsible of the high temperature regime, where the low-lying triplet state was increasingly populated in detriment of the singlet state. Below liquid nitrogen temperature, small antiferromagnetic intermolecular interactions manifest and tend to couple the triplet states in such a way that the $S = 1$ spin vectors cancel each other, and a null global magnetization is approached.

One may note that the magnetic measurements for the ferromagnetic compounds **1** and **3** in Figures 6 and 8 exhibit some noise in the low temperature regime. Nevertheless, this feature is fully reproducible and hence cannot be attributed to defects in the sample, which has been further checked in variable

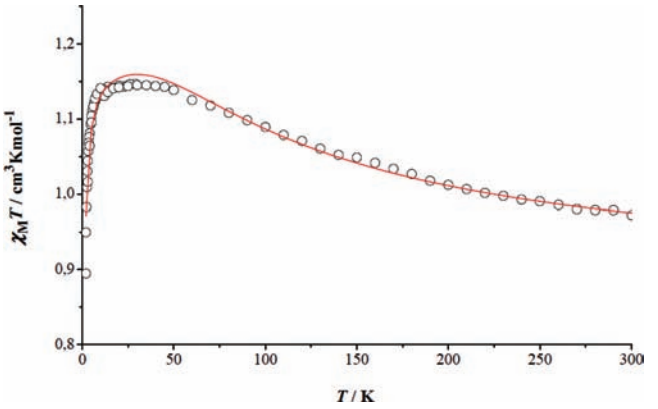

Figure 8. Plot of magnetic susceptibility−temperature product ($\chi_M T$) versus (T) temperature for compound **3**.

field magnetization experiments. Since the noise appears only in the low temperature part of the curve, its influence on the final value of the ferromagnetic coupling constants is rather limited. Unfortunately, it is very difficult to trace the origin of the noise, and a possible explanation is the presence of some magnetic impurities below the detection limit of our equipment.

Compounds **4**−**6** show a shape of the $\chi_M T$ vs T curves which is typical of antiferromagnetically coupled Cu(II) pairs. At room temperature, the $\chi_M T$ values are 0.81, 0.83, and 0.86 cm^3Kmol^{-1}, respectively, close to the value expected for two uncoupled Cu(II) ions. On cooling down, $\chi_M T$ decreases slowly to show a strong descent in the 80−20 K region until reaching values near to zero below 10 K. This behavior is illustrated in Figure 9 for compound **4**, as the curves for products **5** and **6** are very similar.

To account for the magnetic behavior of the dinuclear Cu(II) complexes **4**−**6** and to evaluate the corresponding coupling constant J, defined as the singlet−triplet splitting, we fitted the experimental susceptibility data using the Bleaney−Bowers equation.[25] For the ferromagnetic compounds **1**−**3**, we corrected the above expression with a mean-field Weiss θ parameter to account for the small antiferromagnetic intermolecular interactions detected in the low temperature region for these

dx.doi.org/10.1021/ic200992z |*Inorg. Chem.* 2011, 50, 10648–10659

ferromagnetic dinuclear complexes:

$$\chi_M(T-\theta) = \frac{N\beta^2 g^2}{k_B}\frac{2e^{J/k_BT}}{1+3e^{J/k_BT}} \quad (3)$$

For compound **1**, as there is no unambiguous way to separate the exchange contributions of each dinuclear cation, the assumption of equal coupling constants was imposed in the procedure. Best-fit parameters were obtained by minimization of the error function $R = \Sigma\{[(\chi_M T)_{calc} - (\chi_M T)_{exp}]^2/(\chi_M T)_{exp}^2\}$, and results are shown in Table 2. It is worth noting that magnetic data and fitting results for ferromagnetic compounds **1** and **3** are not quite accurate, mainly due to both the small amount of pure samples available (30 and 60 mg, respectively) for the applied magnetic field and available equipment. Likewise, one must also consider the intrinsic low accuracy and overparametrization problems involving the fitting of ferromagnetically coupled Cu(II)−Cu(II) systems with rather large molecular weights. Note that in the antiferromagnetic compounds $\chi_M T$ ranges from 0 to 0.8 whereas in the case of the ferromagnetic ones it ranges from 0.9 to 1.2 only. The much shorter range $\chi_M T$ leads to a more difficult fitting to the magnetic model, especially because here one has one additional parameter in the fitting, the intermolecular Curie−Weiss temperature. Nevertheless, the g values obtained from the fitting are consistent with those determined by EPR and also reported in Table 2. This provides further support of the accuracy of the J values thus obtained which are discussed below.

The experimental J values for class B compounds **1**, **2**, and **3** are +151.2, +104.5, and +98.4 cm^{-1}, respectively. An explanation for such a trend can be made in terms of countercomplementary effect between the hydroxo bridge which generates ferromagnetic interaction due to the orbital orthogonality and one triatomic bridge in *syn,syn* equatorial−equatorial configuration which usually contributes to a weak antiferromagnetic interaction. The experimental results of magnetic properties (J values) and structural data are summarized in Table 3 for class B compounds **1**−**3**.

The magnetic properties of present class F compounds show a weak antiferromagnetic interaction with the J values of −39.4, −39.7, and −31.4 cm^{-1} for **4**, **5**, and **6**, respectively. An explanation can also be made invoking the countercomplementary effect between the monoatomic bridge and the triatomic bridge in *syn*−*syn* configuration. As there are two triatomic bridges, the dominant (weak) antiferromagnetic interaction is observed for all three compounds. On the other hand, the known class F compound **XV** shows the weak ferromagnetic interaction (J = +10.13 cm^{-1})[8] as expected from the presence of two monoatomic bridges with bridging angles of 102.7(2) and 86.8(2)° and one triatomic bridge. Furthermore, in **XV**, these angles result in the increase of the magnetic orbital orthogonality as compared to the bridging angles of 109.7(1)°, 109.5(1)°, and 108.3(1)° for **4**−**6**, respectively. Magnetic data of all class F compounds is summarized in Table 4.

Theoretical Study of Magnetic Coupling. In order to investigate the magneto-structural correlations for triply bridged dinuclear Cu(II)−Cu(II) molecular systems and to compare the performance of several exchange-correlation density functional potentials in predicting their magnetic coupling constants, we have estimated the singlet−triplet gap through a series of DFT calculations. These are all of hybrid type since it is now well established that pure functional based on the local density approach (LDA) or any of the different generalized gradient approaches (GGAs) largely overestimate the magnitude of the magnetic coupling constants.[26,27] This is not the case with hybrid functional although agreement with experiment required a careful analysis of the fraction of nonlocal Fock exchange included in the exchange potential. Therefore, a series of calculations has been carried out for compounds **1**−**6** using the well-known and widely used stand-alone hybrid functionals BHandHLYP and B3LYP derived from the GGA potentials,[28,29] M06 and M06-2X from the meta GGA functionals family,[30−32] and HSE[33] and LC-ωPBE[34] from the range-separated family recently introduced by Scuseria and co-workers.

Here, let us just recall that the popular B3LYP hybrid-DFT functional incorporates 20% of Fock exchange and a 80% of Becke gradient corrected form of the exchange potential, together with a gradient corrected correlation potential. This method exhibits a good performance in the quantitative description of main group thermochemistry[35] but presents some problems when studying the magnetic coupling of open shell systems such as transition metal polynuclear complexes, where magnetism is strongly dominated by electron exchange and both dynamical and nondynamical correlation effects.[27,28] Like B3LYP, the BHandHLYP is a hybrid-DFT method derived from the GGA but, in this case, the mixture of HF and LDA is 50%:50% and performs better for calculating the magnetic coupling in some systems. The M06 family of meta GGA functionals includes the density, its gradient, and an additional term better approximating the kinetic density potential. The most representative functionals of this family are the M06 and M06-2X, which include 27% and 54% of HF exchange, respectively, although the latter has been optimized for main group chemistry calculations. The performance of the M06 family in

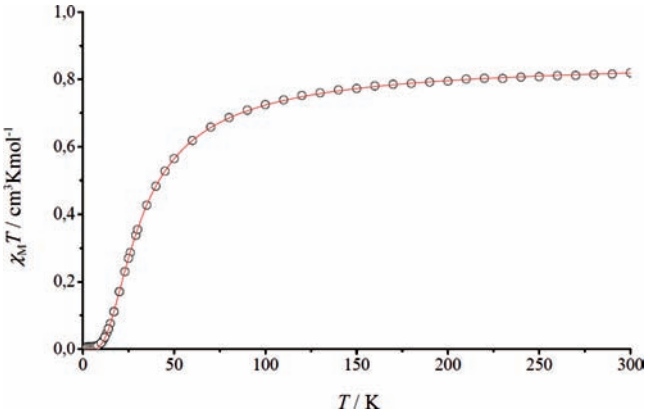

Figure 9. Plot of magnetic susceptibility−temperature product ($\chi_M T$) versus (T) temperature for compound **4**.

Table 2. Experimental Normal and Half-Field (at 20 K) EPR Signals and Best-Fit Susceptibility Data to eq 3 (g_{iso}, J_{exp}, and θ) for Compounds 1−6

Compound	g	$g_{1/2}$	g_{iso}	J_{exp} (cm^{-1})	θ (K)	R ($\times 10^{-4}$)
1	2.014	4.370	2.19 ± 0.01	+151.2 ± 6.0	−0.62 ± 0.02	1.6
2	2.065	4.427	2.20 ± 0.01	+104.5 ± 3.5	−0.59 ± 0.02	1.2
3	2.093	4.396	2.17 ± 0.01	+98.4 ± 3.2	−0.43 ± 0.02	1.8
4	2.126	4.325	2.14 ± 0.01	−39.4 ± 0.2		0.2
5	2.118	4.375	2.17 ± 0.01	−39.7 ± 0.1		0.1
6	2.119	4.311	2.17 ± 0.01	−31.4 ± 0.5		0.6

dx.doi.org/10.1021/ic200992z |*Inorg. Chem.* 2011, 50, 10648–10659

Table 3. Structural and Magnetic Data for Class B Triply-Bridged Dinuclear Copper(II) Compounds[a]

Compound[b]	Geom[c]	τ	ϕ	γ	Class	Cu···Cu	Cu−X		Cu−OH−Cu	J_{exp}	ref[b]
							Axial	Equatorial			
$\{[Cu_2(phen)_2(\mu\text{-}OH)(\mu\text{-}OH_2)(\mu\text{-}O_2CC(CH_3)_3)](ClO_4)_2\}_2(CH_3CH_2OH)$ (**1**)	SP, SP	0.10, 0.22	117.7, 120.4	9.9, 16.2	B	3.010	2.419, 2.379	1.911−2.015	103.8, 105.3	151.2	pw
		0.08, 0.26		8.8, 21.2		3.034	2.425, 2.369	1.893−2.012			
$[Cu_2(bpy)_2(\mu\text{-}OH)(\mu\text{-}O_2CCH_2CH_3)(\mu\text{-}O_2SOCF_3)](CF_3SO_3)(DMF)_{0.5}$ (**2**)	SP, SP	0.14, 0.15	154.8	11.2, 11.8	B	3.341	2.351, 2.354	1.906−2.019	122.3	104.5	pw
$[Cu_2(phen)_2(\mu\text{-}OH)(\mu\text{-}OH_2)(\mu\text{-}O_2CCH_2CH_3)](NO_3)_2$ (**3**)	SP, SP	0.19, 0.21	122.3	14.6, 12.2	B	3.026	2.344, 2.368	1.925−2.029	103.6	98.4	3, pw
$[Cu_2(dpyam)_2(\mu\text{-}OH)(\mu\text{-}OH_2)(\mu\text{-}O_2CCH_3)](S_2O_8)$ (**II**)	SP, SP	0.43	164.4	40.4	B	3.124	2.414	1.911−2.023	109.6	n.d.	3
$[Cu_2(bpy)_2(\mu\text{-}OH)(\mu\text{-}OH_2)(\mu\text{-}O_2CCH_3)](NO_3)_2$ (**III**)	SP, SP	0.21, 0.19	120.5	14.5, 11.6	B	3.049	2.347, 2.460	1.938−2.017	104.0	n.d.	3
$[Cu_2(phen)_2(\mu\text{-}OH)(\mu\text{-}OH_2)(\mu\text{-}O_2CCH_3)](BF_4)_2\cdot 0.5H_2O$ (**IV**)	SP, SP	0.21, 0.16	114.6	17.0, 8.6	B	3.002	2.374, 2.390	1.925−2.008	102.1	120.8	3
$[Cu_2(bpy)_2(\mu\text{-}OH)(\mu\text{-}OH_2)(\mu\text{-}O_2CCH_3)](ClO_4)_2$ (**VI**)	SP, SP	0.14, 0.25	118.1		B	3.035	2.379, 2.405	2.006−2.010	103.8	38.6	3
$[Cu_2(phen)_2(\mu\text{-}OH)(\mu\text{-}OH_2)(\mu\text{-}O_2CCH_3)](ClO_4)_2$ (**VII**)	SP, SP	0.02, 0.14	113.8	16.4, 8.2	B	2.989	2.360, 2.375	1.933−2.020	101.3	120.0	3
$[Cu_2(bpy)_2(\mu\text{-}OH)(\mu\text{-}OH_2)(\mu\text{-}O_2CCH_2CH_3)](ClO_4)_2$ (**VIII**)	SP, SP	0.20, 0.16	120.1	15.0, 10.9	B	3.037	2.382, 2.415	1.920−2.005	104.5	148.9	3
$[Cu_2(bpy)_2(\mu\text{-}OH)(\mu\text{-}O_2CCH_3)(\mu\text{-}Cl)]Cl\cdot 8.5H_2O$ (**IX**)	SP, SP	0.41, 0.28	123.0	27.4, 18.9	B	3.040	2.632, 2.657	1.936−2.029	103.3	145.3	3

[a] Geom stands for the coordination of Cu(1) and Cu(2); τ is the aggregate Addisson for Cu(1)/Cu(2) and Cu(3)/Cu(4) pairs, and ϕ is the angle between basal planes and γ the tetrahedral twist angle, both in degrees. Cu···Cu and Cu−X distances are in Å and Cu−OH−Cu angles in degrees. J_{exp} is the experimentally derived magnetic coupling constant in cm^{-1}. [b] Abbreviations: bpy = 2,2′-bipyridine; dpyam = di-2-pyridylamine; phen = 1,10-phenanthroline; n.d. = not determined; pw = present work. [c] SP = distorted square pyramid.

describing magnetic coupling in Cu(II) dinuclear complexes has been examined by Valero et al. and found to provide a systematic improvement over B3LYP.[17]

Nevertheless, most hybrid functionals fail to correctly describe the asymptotic decay of the exchange potential in insulator molecular systems, which is found extremely slow ($-c/r$ versus the expected $1/r$ trend, c being the fraction of nonlocal exchange). This effect delocalizes in excess the spin density of the paramagnetic centers across the ligands and results on increased coupling constants. In order to solve these problems, Vydrov and Scuseria implemented a long-range corrected hybrid functional (denoted as LC-ωPBE), which restores the proper asymptotic limit using the HF exchange to describe the long-range electron−electron interactions, whereas a GGA functional is used to describe the short-distance interactions in a gradual way:

$$E_{xc}^{LC-\omega PBE}(\omega) = E_x^{LR-HF}(\omega) + E_x^{SR-PBE}(\omega) + E_c^{PBE} \quad (4)$$

The standard value of $\omega = 0.40{a_0}^{-1}$ provides an excellent performance, and it is the one used in this work. Likewise, Heyd, Scuseria, and Ernzerhorf presented a short-range corrected HSE hybrid[34] for the correct description of semiconducting or metallic periodic bulk systems: it avoids the problems found when treating the HF exchange in periodic calculations for semiconductor or metallic systems by switching it on at short electron−electron distances, whereas at long electron−electron distances the PBE functional is exclusively used:

$$E_{xc}^{HSE}(\omega) = aE_x^{LR-HF}(\omega) + (1-a)E_x^{SR-PBE}(\omega) + E_x^{LR-PBE}(\omega) + E_c^{PBE} \quad (5)$$

In this case, the value of $\omega = 0.11{a_0}^{-1}$ has been shown to be the most appropriate, so the HSE06 (the recommended version of the full Heyd−Scuseria−Ernzerhof functional) stand alone functional has been chosen for the calculations performed in this work. The performance of range separated functional in describing magnetic coupling has been recently explored[18] using the same open shell database employed by Valero et al.[17] whereas Phillips and Peralta studied systematically the effect of the range separation ω parameter on the calculated J values.[19]

To obtain a more complete open-shell database of systems involving two unpaired electrons and to further investigate the performance of these recently developed functionals, we have also carried out calculations for the similar series of triply bridged dinuclear Cu(II) compounds studied previously[9] using now the meta and range-separated functionals above-mentioned. To avoid any possible misleading arising from the numbering of the different compounds, those corresponding to compounds studied in previous work are referred to in roman numbers (i.e., compound **4** in ref 9 is compound **IV** here).

In all cases, the molecular structure of the dinuclear complexes has been extracted from the experimentally determined crystallographic structures, except in the cases of compounds **1**, **XII**, and **XIII**, where the position of the hydrogen atom belonging to the OH bridging group was not consistent with the typical bond length and bridging mode of this group and hence adjusted to d(O−H) = 0.90 Å and to a O−H bond forming an angle of aprox. 40° with the vector normal to the Cu−O(H)−Cu plane. All the remaining atom positions were taken from the crystallographic data.

Following the procedure described above and the basis set and computational details given in the corresponding section below, we have computed the singlet−triplet gap for compounds **1**−**6**.

Table 4. Structural and Magnetic Data for Class F Triply-Bridged Dinuclear Copper(II) Compounds[a]

Compound[b]	Geom[c]	τ	γ	Class	Cu···Cu	Cu−O−Cu	J_{exp}	ref[b]
$[Cu_2(bpy)_2(\mu\text{-}OCOPh)(\mu\text{-}O_2CPh)_2](ClO_4)$ (**4**)	SP, interm.	0.38, 0.52	30.1	F1	3.386	109.7	−39.4	pw
$[Cu_2(bpy)_2(\mu\text{-}OCOPh)(\mu\text{-}O_2CPh)_2](BF_4)$ (**5**)	SP, interm.	0.39, 0.52	30.6	F1	3.386	109.5	−39.7	pw
$[Cu_2(bpy)_2(\mu\text{-}OCOPh)(\mu\text{-}O_2CPh)_2](PF_6)$ (**6**)	SP, interm.	0.35, 0.50	28.0	F1	3.384	108.3	−31.4	pw
$[Cu_2(dpyam)_2(\mu\text{-}OCOCH_3)(\mu\text{-}O_2CCH_3)(\mu\text{-}OH)](PF_6)(H_2O)$ (**XV**)	SP, interm.	0.32, 0.51	25.3	F2	2.988	102.7, 86.8	10.13	8

[a] All abbreviations, symbols, and units are as in Table 3. [b] Abbreviations: bpy = 2,2′-bipyridine; dpyam = di-2-pyridylamine; pw = present work. [c] SP = distorted square pyramidal. interm. = intermediate five coordinated geometry.

In order to obtain a more complete database, we have also considered the structurally characterized compounds **I**, **IV**, and **VI**−**XIV** studied in previous work.[9] Calculations have been carried out using the B3LYP and BHandHLYP hybrid functionals, the M06 and M06−2X hybrid meta-GGA functionals, and the HSE and LC-ωPBE range separated functionals. The results, compared to experimental structural and magnetic values, are listed in Table 5. Before describing the calculated values, it is worth to recall that the antiferromagnetic triply bridged compounds **4**−**6** have one of the Cu(II) ions in a square-pyramidal (SP) environment and the other in a mainly trigonal-bipyramidal (TBP) pentacoordination, and hence, together with the ferromagnetic compound **XV**, they can be classified into the class F compounds (see Scheme 1 and ref 8). In the present compounds (see Scheme 2c), the main interaction between the magnetic orbitals occurs through the two *O,O′*-carboxylato bridges, while the monodentate bridging benzoate lies in the apical position of the SP, thus not participating in the superexchange interactions. For this reason, there are no countercomplementary effects through this ligand and only the antiferromagnetic pathways through both bidentate carboxylates remain active. We classify this type of triply bridged antiferromagnetic di-Cu(II) compounds as subclass F1. On the other hand, the ferromagnetic complexes **1**−**3** consist of two Cu(II) ions in a pentacoordinated square-pyramidal (SP) environment in which two basal positions are occupied by two bidentate terminal amines, and the other two are bonded to a μ-hydroxo and a bidentate μ-*O,O′*-carboxylato bridging ion, respectively. The apical positions share the third bridging ligand, which is a monodentate water molecule for compounds **1** and **3**, but a μ-*O,O′*-trifluoromethanesulphonate ion for **2**. According to previous work,[3] they can be classified into triply bridged di-Cu(II) class B compounds (Scheme 2b). This molecular structure fixes the magnetic orbitals (and the spin density of the triplet state) over the $d_{x^2-y^2}$ Cu atomic orbitals and the oxygen donors of the basal bridging ligands that thorough the countercomplementary effect between the carboxylato and the hydroxo basal bridges resulting in a moderately large ferromagnetic interaction.[4] As can be seen in Scheme 2b, the bridging ligands in apical position do not contribute to the magnetic superexchange, although in **2**, its triatomic nature is responsible for the opening of both the interbasal and Cu−O(H)−Cu angles up to 154.8 and 122.3 degrees respectively, due to its steric effect.

In previous work, a trend between the calculated B3LYP and BHHLYP magnetic coupling constants and the aggregate Addison's parameter was identified. Including the calculated values for the three new class B compounds (filled marks) into the plot of the B3LYP and BHHLYP calculated *J* values vs the aggregate Addison's parameter (Figure 10), one can readily see that that **3** lies close to the regression lines, whereas calculated values for **1** are rather higher and for **2** significantly lower. Nevertheless, if new regression lines are plotted which include the new compounds into the fitting, one can observe that they are almost identical with that previously published, except for the rather lower quality of the actual regression coefficients. For these new compounds, neither of these two functionals predict the correct order of intensities in the experimental coupling constants (see Table 5), although the three J_{exp} values lie inside the theoretical intervals defined by the BHHLYP and B3LYP methods, a trend already observed in previous work.[9]

Table 5. Calculated Values of the Coupling Constant *J* (in cm^{-1}) for Compounds 1−6, I, IV, and VI−XV Using Hybrid and Screened Functionals, Compared to Experimental Magnetic Values[a]

		J_{calc}						
Compound	τ_{aggr}	M06−2X	BHHLYP	LC-ωPBE	HSE	B3LYP	M06	J_{exp}
1	0.33	80.2	98.8	***166.0***	180.1	208.0	285.1	151.2
2	0.29	44.3	56.4	87.5	***100.5***	114.1	178.6	104.5
3	0.40	70.0	***85.7***	145.0	156.8	181.4	253.9	98.4
I		97.9	***125.5***	183.7	194.0	220.3	306.8	112.7
IV	0.37	64.9	80.4	***134.6***	145.6	166.6	232.1	120.8
VI	0.37	***67.5***	83.2	135.0	147.3	169.0	235.5	38.6
VII	0.34	65.1	80.5	***135.7***	147.8	169.7	238.8	120.0
VIII	0.37	70.4	87.0	***140.1***	153.8	176.7	248.2	148.9
IX	0.69	56.4	69.4	117.9	126.9	***146.8***	205.3	145.3
X	1.34	66.6	***83.6***	144.1	158.5	185.7	267.5	79.1
XI	1.44	43.6	***78.3***	130.2	140.4	161.3	237.2	79.7
XII	1.28	49.8	***66.2***	109.1	131.3	162.6	267.9	62.5
XIII	1.14	13.9	34.2	***58.0***	78.2	108.1	239.7	47.8
XIV	0.65	***40.1***	57.6	81.1	89.2	99.2	165.8	24.1
XV	0.84	***−5.2***	−15.9	−42.9	−45.3	−78.3	−34.8	10.1
4	0.90	−13.0	−12.2	***−37.2***	−56.1	−73.9	−74.5	−39.4
5	0.91	−13.0	−12.4	***−36.3***	−54.2	−70.9	−71.8	−39.7
6	0.84	−11.7	−11.0	***−31.0***	−47.4	−62.1	−62.5	−31.4

[a] Best theoretical estimates are marked in bold. Roman numbers **I**−**XIV** correlate to the numbering scheme used in ref 9 whereas **XV** is used for compound X in ref 8.

Let us now extend our investigation to the six above-mentioned density functional theory-based methods which in a way correspond to a systematic improvement toward the universal, yet unknown, exact exchange-correlation potential. We will also consider all the triply bridged di-Cu(II) compounds and will center our attention in the results displayed in Table 5, where values in bold indicate the best approximation to the experimental values. From results in Table 5, one can see that calculated values scale through the methods as M06−2X < BHandHLYP < LC-ωPBE < HSE < B3LYP ≪ M06, roughly following the decrease of Hartree−Fock exchange, in line with the work of Martin and Illas, who postulated that for hybrid functionals the magnitude of *J* strongly depends on the exchange potential contribution and it is not largely affected by the choice of the correlation

dx.doi.org/10.1021/ic200992z |*Inorg. Chem.* 2011, 50, 10648–10659

Scheme 2

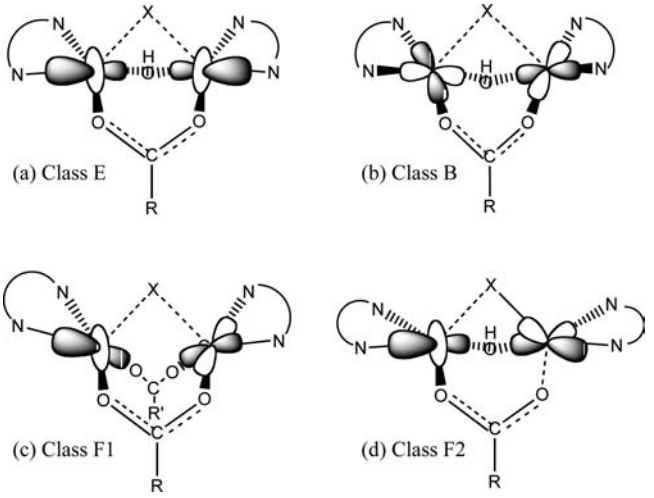

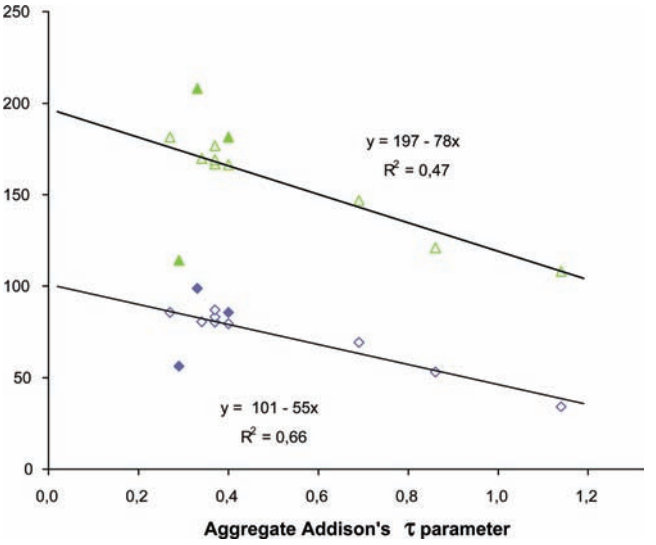

Figure 10. Plot of the B3LYP (triangles) and BHandHLYP (diamonds) calculated J values in cm^{-1} versus the aggregate Addison's parameter for class B compounds. New compounds are marked by filled symbols.

potential.[27,28] It is also interesting to recognize that the calculated values which are closer to experimental ones (marked in bold) are mainly reached by the GGA hybrid BHandHLYP (50% of Fock exchange, 5 hits over 18) and, especially (8 hits over 18), by the range separated LC-ωPBE methods. For the new three antiferromagnetic compounds **4**−**6**, it is undoubtedly clear that LC-ωPBE provides an excellent estimate of the experimental value, in accordance with the results of recent investigations about range-separated hybrid functionals.[18]

With the aim to further verify that the conclusions above are not fortuitous, we expand the compounds database to include a significantly wide range of magnetic interaction in triply bridged di-Cu(II) compounds and employ all the DFT methods. The complete set of results is graphically displayed in Figure 11, where calculated versus experimental singlet−triplet gap values are plotted for each method and compared to the perfect-fitting line in black color. The best slope of the J_{calc} vs J_{exp} regression line still corresponds to the LC-ωPBE functional (1.02), that brings the optimum global behavior on the overall ferro- and antiferromagnetic regions, with a reasonable mean accuracy (+20 cm^{-1} overestimation) and a moderate linear dispersion (R^2 = 0.74). It is worth noting that the second best results are achieved by the HSE screened functional, that was initially designed to deal with metals but which also aims to correct the wrong asymptotic behavior of the PBE functional. For the nonscreened hybrids, the BHandHLYP and B3LYP functionals show the best global behavior, indicating that the presence of a considerable fraction of Fock exchange is a crucial point to correctly describing the energy separation between these spin states.

To round off this work, we finally center our attention on the systems for which our rule-of-thumb does not work. For compounds **2** and **IX**, belonging to class B (Scheme 2b), the experimental J values are higher than those predicted by the LC-ωPBE hybrid, although these are still below those corresponding to the B3LYP limit. On the contrary, compounds **VI** and **XIV** lie even below the M06-2X limit. The case of the only representative of the F2 class (Scheme 2d) of ferromagnetic compounds, **XV**, is still worst: all functionals even fail for predicting the correct sign of J. All three complexes **VI**, **XIV**, and **XV** are characterized by having small ferromagnetic coupling constants (+38, +24, and +10 cm^{-1}, respectively). For the three above-mentioned compounds, all DFT methods explored in this work fail to quantitatively approach the experimental coupling constant, and all exhibit a noticeable excess error: the best approximation (M06-2X) gives an overall 20 cm^{-1} overestimation. For the class F2 compound, all methods predict antiferromagnetic coupling, M06-2X being the one that gives the best approximation (15 cm^{-1} underestimation).

For the only example of ferromagnetic class F2 complex, we can see in the orbital representation drawn in Scheme 2d that the topology of their magnetic orbitals is very different from that of the antiferromagnetic class F1 compounds **4**−**6**. In **XV**, the most intense interaction is between the two lobes of the d_{z^2} (TBP) and $d_{x^2-y^2}$ (SP) lobes through the hydroxo bridge, whereas the bidentate lies in the apical position of the SP coordination of Cu(1), thus debilitating their contribution to the countercomplementary effects and weakening the global ferromagnetic coupling by breaking the delicate balance between opposite interactions.

The fact that small ferromagnetic couplings in systems with countercomplementary bridges are hard to reproduce with the use of monodeterminantal methods was already noticed in previous papers and was attributed to the fact that DFT functions cannot fully account for dynamical electron correlation effects.[36] There, it was suggested that multiconfigurational post Hartree−Fock calculations could be needed to achieve a better fit for these systems, although the need of huge computational resources limited them to the use of complete active space second-order perturbation theory (CASPT2 method) on simplified model systems.[37] Nevertheless, it is the case that an error on the J sign, as we have observed in the present paper, was not detected. In fact, the delicate balance of the interelectronic interactions in such a feebly ferromagnetically coupled compound is still not described with enough accuracy, but the tailoring of new and

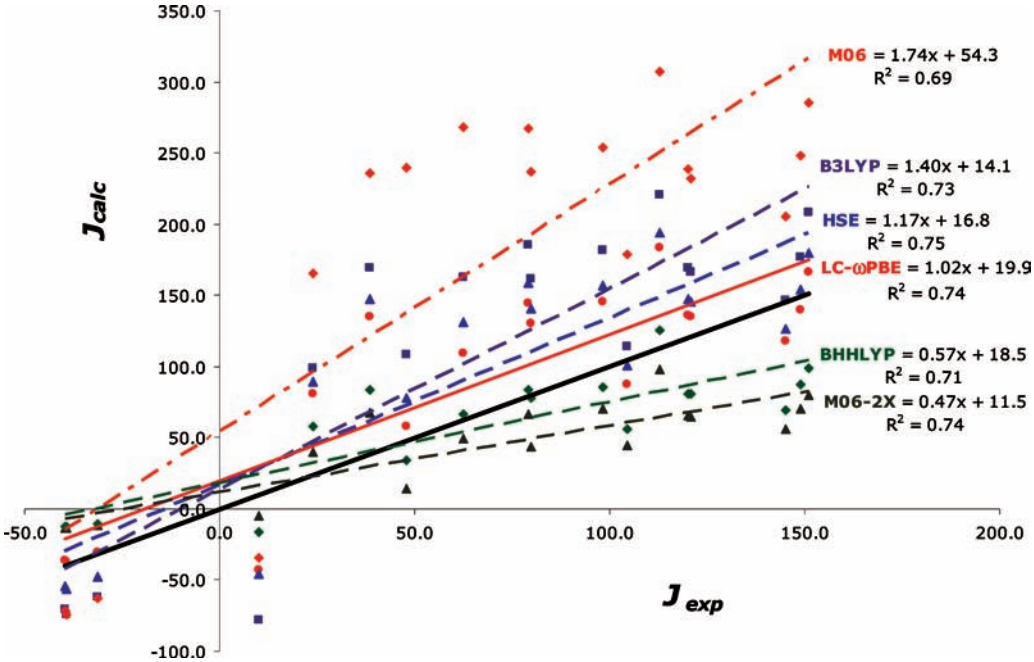

Figure 11. Calculated (J_{calc}) vs experimental (J_{exp}) values (in cm^{-1}) of the singlet−triplet gap for the Cu dinuclear complexes in Table 5. The black line corresponds to the perfect fit.

promising hybrid methods seems to tell us that we are in the correct way.

CONCLUSIONS

Hetero triply bridged dinuclear Cu(II) compounds form a very interesting class of systems with a broad range of values for the magnetic coupling constant. Here, we extend our knowledge of these materials by studying experimentally and theoretically the magnetic properties of two newly synthesized, $\{[Cu_2(phen)_2(\mu\text{-}OH)(\mu\text{-}OH_2)(\mu\text{-}O_2CC(CH_3)_3)](ClO_4)_2\}_2(CH_3CH_2OH)$ (**1**) and $[Cu_2(bpy)_2(\mu\text{-}OH)(\mu\text{-}O_2CCH_2CH_3)(\mu\text{-}O_2SOCF_3)](CF_3SO_3)(DMF)_{0.5}$ (**2**), one previously reported $[Cu_2(phen)_2(\mu\text{-}OH)(\mu\text{-}OH_2)(\mu\text{-}O_2CCH_2CH_3)](NO_3)_2$ (**3**) class B compound, and three new homo triply bridged dinuclear Cu(II), $[Cu_2(bpy)_2(\mu\text{-}OCOPh)(\mu\text{-}O_2CPh)_2]X$ with $X = ClO_4^-$ (**4**), BF_4^- (**5**), and PF_6^- (**6**), class F compounds. Compounds **1**−**3** are found to be ferromagnetically coupled whereas compounds **4**−**6** are antiferromagnetically coupled. Values for the magnetic coupling constants have been derived by appropriate fitting of the experimental susceptibility data using the Bleaney−Bowers equation.[26]

The origin of the magnetic interactions and the magnitude of the magnetic coupling have been analyzed by means of state of the art density functional theory-based calculations. Moreover, it is shown that, for class B and E compounds, the aggregate Addison's parameter provides a possible magneto-structural correlation, confirming the conclusion from previous work on similar compounds.[9]

From the whole set of DFT calculations carried out in the present work including the newly characterized compounds **1**−**6** and including data from previous work on other Cu(II) dinuclear complexes,[9] one can conclude that the ideas behind range-separated functionals are on the right track to derive electronic structure methods that have to deal with subtle energy differences between well-defined states in molecular systems. In particular, the fact that the slope of the experimental versus calculated J values is close to 1 for the LC-ωPBE provides a strong indication of the predictive character of this new density functional theory method.

ASSOCIATED CONTENT

Supporting Information. A more detailed description of the crystal structure of compounds **1** to **6**. This material is available free of charge via the Internet at http://pubs.acs.org. CCDC numbers 787996, 787997, 787998, 787999, and 788000 contain the supplementary crystallographic data for compounds **1**, **2**, and **4**−**6**. These data can be obtained free of charge via http://www.ccdc.cam.ac.uk/conts/retrieving.html or from the Cambridge Crystallographic Data Centre, 12 Union Road, Cambridge CB2 1EZ, UK; fax: (+44) 1223−336−033; or e-mail: deposit@ccdc.cam.ac.uk.

AUTHOR INFORMATION

Corresponding Author

*E-mail: sujittra@kku.ac.th (S.Y.); francesc.illas@ub.edu (F.I.). Phone: +66-4320-2222 ext. 12243 (S.Y.); +34934021229 (F.I.). Fax: +66-4320-2373(S.Y.); +34934021231 (F.I.).

ACKNOWLEDGMENT

Financial support has been provided by the Spanish MICINN (Grant FIS2008-02238), Generalitat de Catalunya (Grants 2009SGR1041 and XRQTC), the Thailand Research Fund (Grant BRG5280012), the Royal Golden Jubilee Ph.D. Program (Grant PHD/0234/2550), the Higher Education Research Promotion and National Research University Project of Thailand, Office of the Higher Education Commission, through the Advanced Functional Materials Cluster of Khon Kaen University

and the Center of Excellence for Innovation in Chemistry (PERCH-CIC), Commission on Higher Education, Ministry of Education. Part of the computational time provided by the Centre de Supercomputació de Catalunya (CESCA) is also gratefully acknowledged.

REFERENCES

(1) Kahn, O. *Molecular Magnetism*; VCH Publishers: New York, 1993.
(2) Carlin, R. L. *Magnetochemistry*; Springer: Berlin, 1986.
(3) Youngme, S.; Phatchimkun, J.; Wannarit, N.; Chaichit, N.; Meejoo, S.; van Albada, G. A.; Reedijk, J. *Polyhedron* **2008**, *27*, 304–318.
(4) Christou, G.; Perlepes, S. P.; Libby, E.; Folting, K.; Huffman, J. C.; Webb, R. J.; Hendrickson, D. N. *Inorg. Chem.* **1990**, *29*, 3657–3666.
(5) Chailuecha, C.; Youngme, S.; Pakawatchai, C.; Chaichit, N.; Van Albada, G. A.; Reedijk, J. *Inorg. Chim. Acta* **2006**, *359*, 4168–4178.
(6) Youngme, S.; Chailuecha, C.; Van Albada, G. A.; Pakawatchai, C.; Chaichit, N.; Reedijk, J. *Inorg. Chim. Acta* **2004**, *357*, 2532–2542.
(7) Youngme, S.; Chailuecha, C.; Van Albada, G. A.; Pakawatchai, C.; Chaichit, N.; Reedijk, J. *Inorg. Chim. Acta* **2005**, *358*, 1068–1078.
(8) Chowdhury, H.; Rahaman, S. K.; Ghosh, R.; Sarkar, S. K.; Corbella, M.; Ghosh, B. K. *Inorg. Chem. Commun.* **2006**, *9*, 1276–1280.
(9) Costa, R.; Moreira, I. de P. R.; Youngme, S.; Siriwong, K.; Wannarit, N.; Illas, F. *Inorg. Chem.* **2010**, *49*, 285–294.
(10) Siemens SAINT, *Version 4 Software Reference Manual*; Siemens Analytical X-ray Systems, Inc.: Madison, WI, USA, 1996.
(11) Sheldrick, G. M. SADABS: *Program for Empirical Absorption correction of Area Detector Data*; University of Göttingen: Göttingen, Germany, 1996.
(12) Bruker, XSHELL, *Version 6.12 Reference Manual*; Bruker AXS, Inc.: Madison, WI, USA, 1999.
(13) Illas, F.; Moreira, I. de P. R.; Bofill, J. M.; Filatov, M. *Phys. Rev. B* **2004**, *70*, 132414.
(14) Illas, F.; Moreira, I. de P. R.; Bofill, J. M.; Filatov, M. *Theor. Chem. Acc.* **2006**, *115*, 587–597.
(15) Moreira, I. de P. R.; Costa, R.; Filatov, M.; Illas, F. *J. Chem. Theory Comput.* **2007**, *3*, 764–774.
(16) Caballol, R.; Castell, O.; Illas, F.; Malrieu, J. P.; Moreira, I. de P. R. *J. Phys. Chem. A* **1997**, *101*, 7860–7866.
(17) Valero, R.; Costa, R.; Moreira, I. de P. R.; Truhlar, D. G.; Illas, F. *J. Chem. Phys.* **2008**, *128*, 114103.
(18) Rivero, P.; Moreira, I. de P. R.; Illas, F.; Scuseria, G. E. *J. Chem. Phys.* **2008**, *129*, 184110.
(19) Phillips, J. J.; Peralta, J. E. *J. Chem. Phys.* **2011**, *134*, 034108.
(20) Ruiz, E.; Alemany, P.; Alvarez, S.; Cano, J. *J. Am. Chem. Soc.* **1997**, *119*, 1297–1303.
(21) Ruiz, E. *J. Comput. Chem.* **2011**, *32*, 1998–2004.
(22) Frisch, M. J. et al. *Gaussian 09*, Revision **A.1**; Gaussian, Inc.: Wallingford CT, 2009.
(23) Nakamoto, K. *Infrared and Raman Spectra of Inorganic and Coordination Compounds: Part B*, 5th ed.; Wiley: New York, 1997.
(24) Hathaway, B. J., Wilkinson, G., Gill, R. D., McCleverty, J. A., Eds. *Comprehensive Coordination Chemistry*; Pergamon Press: Oxford, 1987; Vol. 5.
(25) Bleaney, B.; Bowers, K. D. *Proc. R. Soc. London, Ser. A* **1952**, *97*, 451–465.
(26) Martin, R. L.; Illas, F *Phys. Rev. Lett.* **1997**, *79*, 1539–1542.
(27) Illas, F.; Martin, R. L. *J. Chem. Phys.* **1998**, *108*, 2519–2527.
(28) Becke, A. D. *J. Chem. Phys.* **1993**, *98*, 5648–5652.
(29) Stephens, P. J.; Devlin, F. J.; Chabalowski, C. F.; Frisch, M. J. *J. Phys. Chem.* **1994**, *98*, 11623–1627.
(30) Zhao, Y.; Truhlar, D. G. *J. Chem. Phys.* **2006**, *125*, 194101.
(31) Zhao, Y.; Truhlar, D. G. *J. Phys. Chem. A* **2006**, *110*, 13126–13130.
(32) Zhao, Y.; Truhlar, D. G. *Theor. Chem. Acc.* **2008**, *120*, 215–241.
(33) Heyd, J.; Scuseria, G. E.; Ernzernhof, M. *J. Chem. Phys.* **2003**, *518*, 8207–8215. **2006**, *124*, 219906(E).
(34) Vydrov, O. A.; Scuseria, G. E. *J. Chem. Phys.* **2006**, *125*, 234109.
(35) Zhao, Y.; Truhlar, D. G. *Chem. Phys. Lett.* **2011**, *502*, 1–13.
(36) López, C.; Costa, R.; Illas, F.; de Graaf, C.; Turnbull, M. M.; Landee, C. P.; Espinosa, E.; Mata, I.; Molins, E. *Dalton Trans.* **2005**, *13*, 2322–2330.
(37) de Graaf, C.; Sousa, C.; Moreira, I. de P. R.; Illas, F. *J. Phys. Chem. A* **2001**, *105*, 11371–11378.